Impact of concomitant Y and Mn substitution on superconductivity in $La_{1-y}Y_yFe_{1-x}Mn_xAsO_{0.89}F_{0.11}$

Rhea Kappenberger,[1,2,*] Franziska Hammerath,[1,2] Pierre Rousse,[1] Mesfin Asfaw Afrassa,[1,3] M. Hossein Haghighi,[1] Sirko Kamusella,[2] Giacomo Prando,[1,5,7] Gianrico Lamura,[4] Anja U. B. Wolter,[1] Matteo Moroni,[5] Samuele Sanna,[6] Pietro Carretta,[5] Christian Hess,[1,7] Hans-Joachim Grafe,[1] Hans-Henning Klauss,[2] Sabine Wurmehl,[1,2,*] and Bernd Büchner[1,2,7]

[1]*Leibniz Institute for Solid State and Materials Research, 01069 Dresden, Germany*

[2]*Institute of Solid State and Materials Physics, TU Dresden, 01062 Dresden, Germany*

[3]*Adama Science and Technology University, Adama, Ethiopia*

[4]*CNR-SPIN, c/o Dipartimento di Fisica, University of Genoa, Via Dodecaneso 33, 16146 Genova, Italy*

[5]*Dipartimento di Fisica and Unità CNISM di Pavia, I-27100 Pavia, Italy*

[6]*Department of Physics and Astronomy, University of Bologna and CNR-SPIN, via Berti-Pichat 6-2, 40127 Bologna, Italy*

[7]*Center for Transport and Devices, TU Dresden, 01069 Dresden, Germany*

(Received 3 November 2017; published 28 February 2018)

We discuss the impact of concomitant substitution of Fe by Mn and La by Y in optimally F-doped $LaFeAsO_{0.89}F_{0.11}$. Mn has a known poisoning effect on superconductivity which is particularly strong in the La1111 system, where 0.2% of Mn were reported to completely suppress superconductivity. Through isovalent substitution of La by the much smaller Y we are able to inflict chemical pressure on the structure, which we show is stabilizing the superconducting state, resulting in a drastically larger amount of Mn needed to completely quench superconductivity. Interestingly, we find that the lattice parameter c changes significantly even for small amounts of Mn substitution within a series, which is unexpected taking only the differences between ionic radii into account. We discuss our findings in the light of electron localization caused by small amounts of paramagnetic Mn impurities in $La_{1-y}Y_yFe_{1-x}Mn_xAsO_{0.89}F_{0.11}$ also indicated by resistivity and Mößbauer measurements.

DOI: 10.1103/PhysRevB.97.054522

I. INTRODUCTION

The impact of substituting Fe with Mn in the iron pnictide superconductors is quite unique as it has shown to quench superconductivity even in very small substitution amounts. The destructive effect of Mn has been observed not only for the 1111 system [1] but also for several members of the 122 family [2,3]. Mn has one d electron less than Fe and might be considered as a hole dopant, but in contrast to successful hole doping for example in (Ba,K)122, which leads to superconductivity [4], Mn is poisonous to superconductivity in every case that has been investigated so far. Indeed, several methods such as nuclear magnetic resonance (NMR) [5], inelastic neutron scattering [6], and photoemission spectroscopy [7] have ruled out a charge doping of Mn, and its strong effect on superconductivity has been attributed to electron localization [1,8,9]. The detrimental effect of Mn substituting Fe in F-doped La1111 is unusually strong: 0.2% have been found to completely suppress superconductivity [1]—very little compared to, e.g., 4% in optimally F-doped Nd1111 [1] and 8% in optimally F-doped Sm1111 [8,10]. Looking for possible causes for this behavior, the first thing coming to mind is the difference in the ionic radii of the rare earth ions (a noticeable decrease from La to Sm), but La and Sm also show different magnetic behavior. La is nonmagnetic, whereas Sm has paramagnetic properties [11]. This opens the question whether the higher Mn tolerance of Sm1111 can be attributed simply to the smaller radius or whether this behavior is correlated to the magnetic nature of Sm.

In order to study the influence of the size of the rare earth ion in the 1111 family in more detail, La substitution by Y in the La1111 system has been investigated [12,13]. This is a case of isovalent substitution, as both La and Y have a charge of +3. However, La^{3+} (116 pm) substitution by Y^{3+} (102 pm) also leads to a shrinking of the lattice which in turn is correlated with an increase of T_c from 26 K to 43 K. It is along the line of arguments that applying pressure increases T_c in LaFeAs(O,F) up to 43 K [14]. Unfortunately, the amount of Y substitution seems to be limited, as the experimental results of Shirage *et al.* [12] and Tropeano *et al.* [13] suggest a thermodynamic limit at about 20% Y. It has been suggested that La1111 is near a quantum critical point (QCP) [15], where very small changes in stoichiometry lead to significant changes of the physical properties. As the influence of impurities seems to be less pronounced in Sm1111 and Nd1111, one can conclude in this scenario that a smaller ion in place of La drives the 1111 system farther away from the QCP.

In this paper, we addressed the question whether the Mn tolerance in the 1111 system is governed by the size of the rare earth ion by concomitantly substituting La by the smaller Y as well as introducing Mn on the Fe position. As Y^{3+} is nonmagnetic, we can simulate the steric effect on the 1111 lattice without the additional magnetic influence stemming from, e.g., Sm. Since an F content of about 11% is generally accepted as optimal doping, the F content of all our samples was fixed to this value. A first sample series with a fixed Mn content of 0.5% was produced, which is already enough

*r.kappenberger@ifw-dresden.de, s.wurmehl@ifw-dresden.de

to suppress superconductivity in $LaFeAsO_{0.89}F_{0.11}$ according to literature [1]. Additionally, the Y content was gradually increased from 0 to 20%. It was observed that the increase in the chemical pressure associated with Y doping caused the recovery of the superconducting state.

For a second sample series, the Y content was fixed at the maximum possible value of 20% and Mn was gradually introduced to get insight on how much Mn the system will tolerate while being subjected to chemical pressure. This sample series has already been subject to ^{19}F-NMR and μSR measurements which showed a less effective suppression of the superconducting ground state by Mn substitution in the presence of Y substitution. Remarkably, magnetic order emerges as soon as the superconducting phase is suppressed [16,17]. Experimental details concerning synthesis and characterization techniques are presented in Sec. II. Section III A contains information about the microstructure and the local composition. Results regarding the structural properties can be found in Secs. IV A (0.5% Mn series) and IV B (20% Y series), all magnetic properties are summed up in Secs. IV C (0.5% Mn series) and IV D (20% Y series). Section IV E contains results obtained by specific heat measurements, whereas results of the resistivity measurements can be found in Sec. IV F. Mößbauer measurements are presented in Sec. IV G. All results are discussed in Sec. V.

II. EXPERIMENTAL DETAILS

Thirty-four polycrystalline $La_{1-y}Y_yFe_{1-x}Mn_xAsO_{0.89}F_{0.11}$ samples in two sample series with nominal values of (i) $x(\mathrm{Mn}) = 0$–0.2 along with $y(\mathrm{Y}) = 0.2$ (referred to as the 20% Y series) and (ii) $y(\mathrm{Y}) = 0$–0.2 and $x(\mathrm{Mn}) = 0.005$ (referred to as the 0.5% Mn series) have been prepared using a two-step solid-state reaction similarly to what is described in Ref. [18]. In the first step, LaAs was prepared from La lumps (Chempur, 99.9%) and As lumps (Chempur, 99.999%) reacting a stoichiometric ratio in an evacuated quartz tube placed in a two-zone furnace. YAs was prepared accordingly (Y from Chempur, 99.9%). In the second step, we used the resulting LaAs and YAs and mixed it with Fe (Alfa Aesar, 99.998%), Fe_2O_3 (Chempur, 99.999%), Mn (Alfa Aesar, 99.9%), and FeF_3 (Alfa Aesar, 97%) in the corresponding stoichiometric ratio. All starting materials were homogenized by grinding in a ball mill. The resulting powders were pressed into pellets under Ar atmosphere using a force of 20 kN and subsequently annealed in an evacuated quartz tube in a two-step annealing process (940 °C for 8 h and 1150 °C for 48 h).

The microstructure and the composition were analyzed by scanning electron microscopy (SEM) on freshly polished polycrystals. We used two different SEMs for the sample characterization: (i) a Philips XL30 equipped with a microprobe analyzer (energy-dispersive x-ray spectrometer, EDX) for semiquantitative elemental analysis, (ii) a Zeiss EVOMA15 with compositional analysis using EDX and wavelength dispersive x-ray spectroscopy (WDX) along with FeS_2, Mn, LaB_6, InAs, CeF_3, and MgO standards for quantification (Oxford Instruments, Inca, and AzTec software). The acceleration voltage applied was 30 kV.

Powder x-ray diffraction was performed using a STOE STADI diffractometer in transmission geometry with Mo-K_{α_1} radiation equipped with a Germanium monochromator and a DECTRIS MYTHEN 1K detector. The samples were either phase pure or contained less than 2 wt% of rare earth arsenide (REAs), RE_2O_3, and REF_3. The data were evaluated with the Rietveld method with Fullprof in the WinPlotR program package [19,20]. The peak shape was assumed to be a pseudo-Voigt function and the refinement included the following aspects: (i) the background, which was linearly extrapolated from 6–10 background parameters, (ii) the scale factors, (iii) the global instrumental parameters (zero-point 2 θ shift and systematic shifts, depending on transparency and off-centering of the sample), (iv) the lattice parameters, and (v) the profile parameters (Caglioti half-width parameters of the pseudo-Voigt function). The texture correction was included using the March-Dollase function.

Magnetization measurements were performed on superconducting quantum interference device magnetometers (SQUID-VSM, MPMS XL-5, and MPMS2) from Quantum Design. The magnetization data was obtained in the temperature range 1.8–40 K applying 10 or 20 Oe in zero-field-cooled (ZFC) and in field-cooled (FC) conditions. We defined T_c as the point where the magnetization is lower than the tangent to the normal state. No demagnetization correction was used.

Mößbauer spectroscopy was performed with a standard Wissel spectrometer in transmission geometry employing a ^{57}Co source with initial activity of 2 GBq and a source line width of 0.105 mm/s. The drive was run in sinusoidal mode minimizing the velocity error. Measurements were performed at room temperature and at 4.2 K for selected samples. Spectra were analyzed using Moessfit [21].

^{19}F NMR measurements have been performed in a static magnetic field of 1.5 T at room temperature on some selected samples. A standard Hahn spin echo sequence was used to measure the NMR signal intensity at room temperature. The repetition rate between subsequent pulse sequences was chosen long enough (5 s) to prevent spin-lattice relaxation effects on the measured signal intensity. Similarly, the time τ which separates the 90° and 180° pulse in the Hahn spin echo sequence was kept constant throughout all measurements (20 μs) to prevent spin-spin-relaxation effects on the measured signal intensity. Thus, the obtained NMR signal intensity is a measure of the number of F atoms in the samples and can be used to control the doping level on a relative scale.

Resistivity measurements were performed in the temperature range 4.3–300 K in a home-made device using a standard four-probe technique. Electrical contacts were made using thin copper wires attached to the sample surface with a silver epoxy.

Specific heat measurements were performed using a heat-pulse relaxation method in a physical property measurement system (PPMS from Quantum Design). The heat capacity of the sample holder (addenda) was determined in zero field and in an external field of 9 T prior to the measurements for the purpose of separating the heat capacity contribution of the sample from the total heat capacity.

III. MICROSTRUCTURE AND LOCAL COMPOSITION

EDX was performed to verify the actual composition both in form of mapping of the elemental distribution over

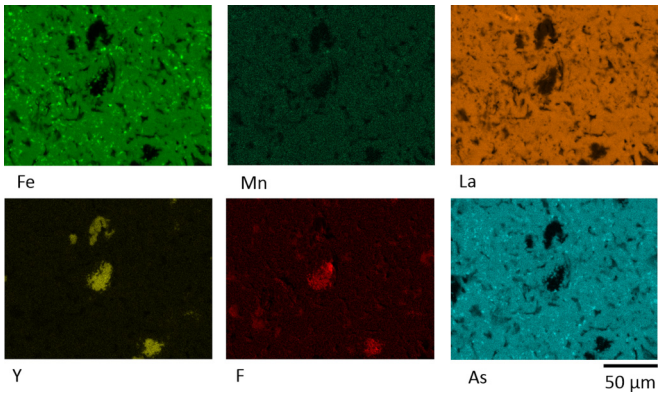

FIG. 1. SEM mapping of Fe, Mn, La, Y, F, and As in a representative sample with 4% Mn and 20% Y.

representative areas as well as in the form of point spectra at several spots of a given sample.

Figure 1 exemplarily shows the elementary distribution maps obtained with SEM of the sample with 4% Mn and 20% Y. A difference in color reflects a difference in composition. A homogenous distribution of all elements can be observed with few exceptions—the darker areas in the Fe, Mn, La, and As mappings correspond to a lighter area in the Y map, which shows that those areas correspond to Y-rich phases. Since the F content is also higher in these areas as reflected by the brighter contour in the F mapping, those secondary phases represent an YF_3 phase, possibly also YOF. It should be noted that the depicted mappings are representative for areas with impurities.

A. 0.5% Mn series

All samples in the 0.5% Mn series have a nominal F content of 11%. The Y content is varied from 0 to 20%. In order to verify the actual composition, the nominal contents of Y and F are plotted as functions of the EDX values in Fig. 2. The Mn content of nominally 0.5% Mn can obviously not be quantified using EDX. The corresponding error bars are estimated from the standard deviations obtained by averaging over several small areas of the sample matrix. The Y content matches quite

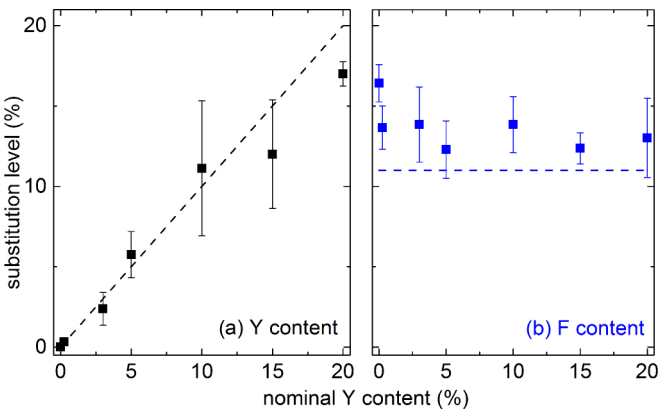

FIG. 2. (a) Y and (b) F content of the 0.5% Mn series as measured by EDX. The dotted lines represent the nominal compositions whereas the dots show the real composition as determined using EDX.

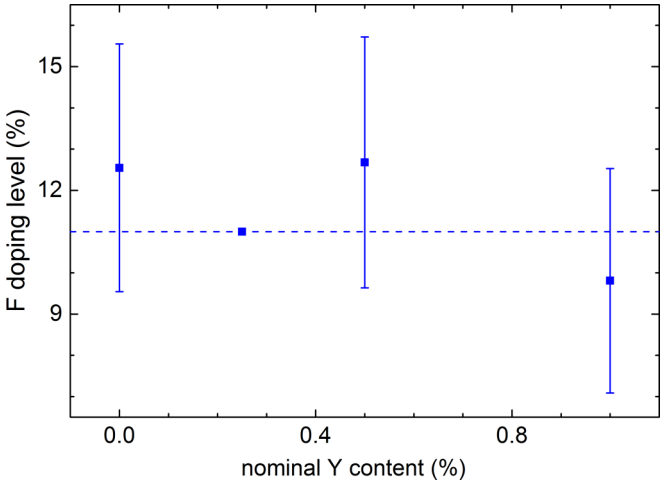

FIG. 3. F-doping level of four samples of the 0.5% Mn series determined by ^{19}F-NMR in 1.5 T. The F-doping amount is calculated relative to the sample with a Y content of 0.25%.

well with the nominal composition. For the F content, EDX shows a scatter from 12–18%; this is caused by significant overlap of the F-Kα line and the Fe-Lα line, also EDX tends to overestimate light elements. In order to further shed light on the actual F content, ^{19}F-NMR measurements have been performed in an applied magnetic field of $\mu_0 H = 1.5$ T on some selected samples to confirm the relative fluorine doping level. Within the error bars, no variation of the intensity of the ^{19}F-NMR resonance line was found, confirming that the intrinsic F content does not differ among the samples within ±3%. This is illustrated in Fig. 3 where the F content of four samples of the 0.5% Mn series is compared. The F content is calculated relative to the sample with a Y content of 0.25%. The error bar includes the consideration of the errors of the measured intensity, the mass of the samples, and the filling factor of the NMR coil. To further elucidate this issue, we also performed WDX (results not shown) on selected samples confirming the EDX results. As our compositional analysis confirms that the sample compositions match the nominal compositions very well, we refer to specific samples of the 0.5% series by their nominal composition.

B. 20% Y series

All samples in this series have a nominal F content of 11% and a nominal Y content of 20%. The Mn content is varied from 0 to 20%. In Fig. 4 the nominal contents of Y, F, and Mn are plotted as a function of the EDX values. The corresponding error bars are estimated from the standard deviations obtained by averaging over several small areas of the sample matrix. Similar to the 0.5% Mn series, the F content is overestimated with this method as discussed in Sec. III B. The Y content is systematically somewhat lower than the desired 20% which reflects that we are near the maximum amount of Y this phase can tolerate before phase segregation happens (see also Tropeano *et al.* [13] and Shirage *et al.* [12]). The Mn content matches the nominal composition very well. Hence, we refer in the following to a specific sample by the nominal composition.

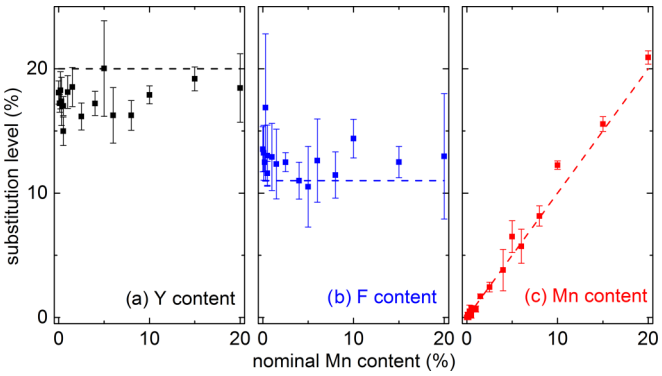

FIG. 4. F, Y, and Mn content of the 20% Y series as measured with EDX.

IV. PHYSICAL PROPERTIES

A. Structural properties of the 0.5% Mn series

Exemplary XRD patterns of samples with 0.5% Mn and 0.5, 3, 10, 15% Y are shown in Fig. 5. Nearly all of the reflections can be indexed based on the space group 129 ($P4/nmm$). However, in some samples we see small additional reflections which can be attributed to LaAs. Figure 6 exemplarily shows the Rietveld refinement of the sample with 0.25% Y as a typical example for this series; the main peak of the secondary phase LaAs is marked with a black circle. The amount of this impurity can be estimated by the Rietveld refinement to be on the order of 1%. Impurities such as YF_3 and YOF which were detected using EDX could not be detected with XRD as their main reflections are obscured by the reflections of the main phase. All patterns and refinements with the respective R_{wp} values are found in the Supplemental Material [24].

The lattice parameters of all samples were also obtained from the structure model: There is no significant change in the lattice parameter a (not shown), however, the lattice parameter c shows a decrease of 0.4% with increasing Y content as seen in Fig. 7, which mimics Vegard's law [22].

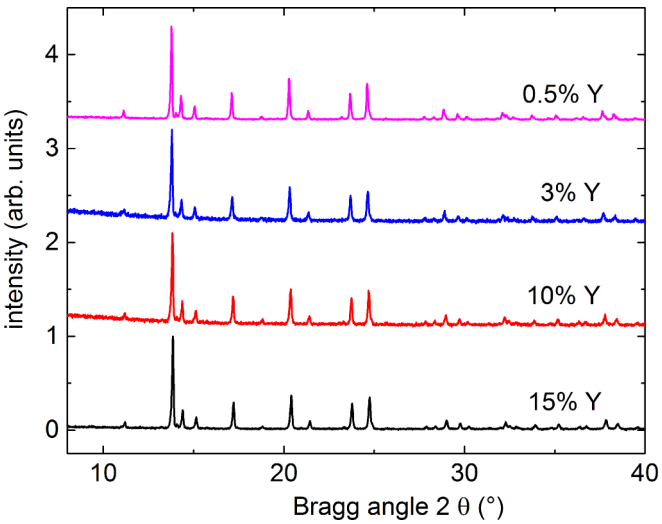

FIG. 5. Exemplary XRD spectra of the 0.5% Mn series with 0.5, 3, 10, 15% Y.

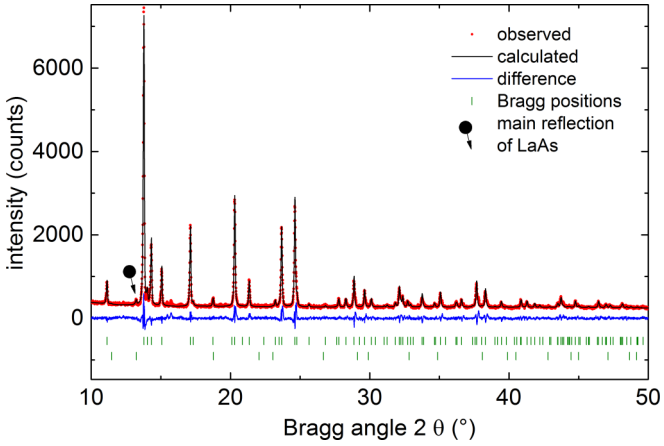

FIG. 6. Exemplary Rietveld refinement on the sample with 0.25% Y and 0.5% Mn. The black dot marks the main peak of the second phase LaAs.

A similar trend upon Y substitution has also been found by Tropeano *et al.* [13] and Shirage *et al.* [12] in samples with no additional Mn substitution. In general, a decrease is expected from a comparison of the ionic radii of La^{3+} (116 pm) [23] and Y^{3+} (102 pm) [23]. Taking a very simplified view on the contribution of the La/Y ionic radius on the c axis as $2 \cdot r(La^{3+})$, the expected decrease of c with a 20% substitution of La by Y amounts to -0.6%, which is reasonably close to the experimental value. It should be noted that there is significant scattering of c. This can be attributed to the very difficult stoichiometry control during the synthesis as only some milligrams of Mn- or Y-containing precursors are used for the samples with low substitution grades, which leads to proportionally large errors regarding the actual composition. Also, small amounts of substitution are not verifiable with EDX as mentioned in Sec. III B.

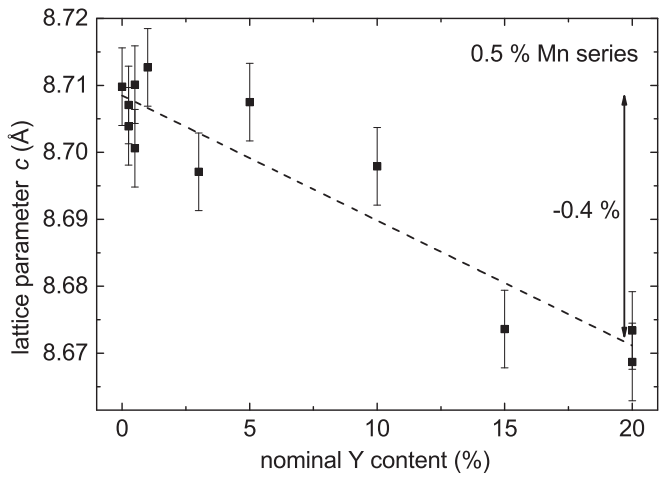

FIG. 7. Linear decrease of the lattice parameter c of the 0.5% Mn series as a function of the nominal Y content. The dotted line is a linear regression with a slope of -0.4%. The error bars were obtained by comparing the values of c for two samples with the same nominal composition.

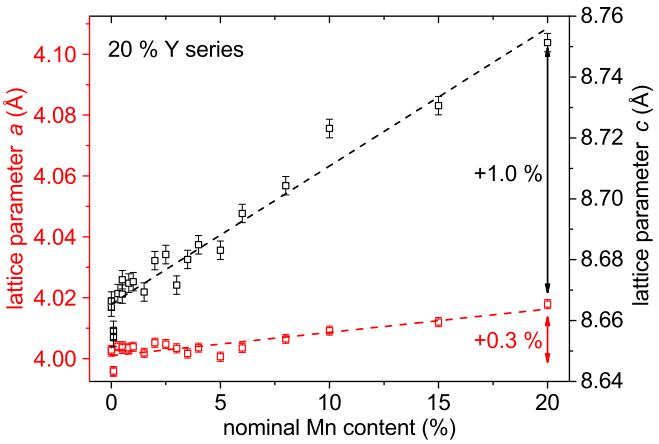

FIG. 8. Linear increase of lattice parameters a (in red) and c (black) as a function of the nominal Mn content in the 20% Y series. The error bars were obtained by comparing the values of a and c for two samples with the same nominal composition.

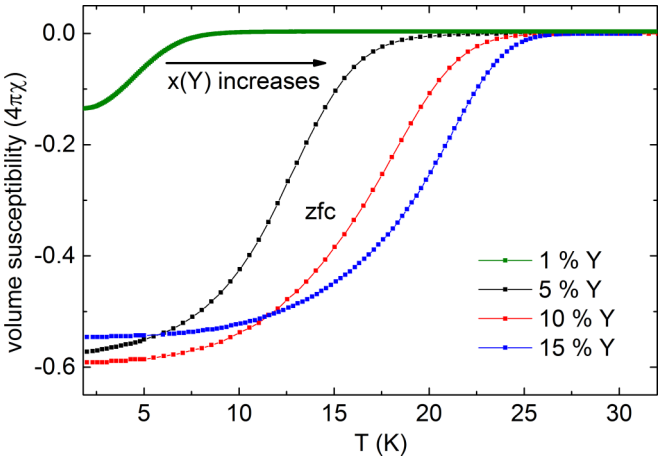

FIG. 9. Magnetic volume susceptibility measured with a field of 20 Oe of four selected samples of the 0.5% Mn series with 1, 5, 10, 15% Y without demagnetization correction.

B. Structural properties of the 20% Y series

In the 20% Y sample series, the lattice parameters were extracted in the same way as described for the 0.5% Mn series in Sec. IV A. All patterns and refinements with the respective R_{wp} values are found in the Supplemental Material [24]. Figure 8 shows that the lattice parameter a increases by 0.3%, whereas the lattice parameter c increases by 1%. The linear trend as such proves that the substitution is successful. A similar behavior of c has been observed in the $BaFe_{2-x}Mn_xAs_2$ system [25]. This increase of the c axis cannot be explained purely by the quite small difference of the ionic radii of Fe^{2+} (63 pm) [23] and Mn^{2+} (66 pm) [23]. Using the simplified calculation mentioned in Sec. IV A, one should expect an increase of c of only about 0.14% when substituting 20% of Fe by Mn. However, other cases such as Rh doping in NaFeAs (where c decreases even though Rh^{2+} is larger than Fe^{2+} [26]) show that c is not determined by the ionic radius of the dopant on the Fe position. A thorough investigation of these phenomena has been done by Johrendt *et al.* [27]. In the present case, the disproportionally large increase of c could hint at electron localization caused by Mn, as this leads to a smaller orbital overlap [28]. Interestingly, the electron localizing Mn seems to strongly counteract the electron doping effect of F as evidenced by the behavior of lattice parameter c. c increases by 0.3% [13] by going from $La_{0.8}Y_{0.2}FeAsO_{0.85}F_{0.15}$ to fluorine-free $La_{0.8}Y_{0.2}FeAsO$, which is an amount of increase in c one can also reach by substituting only 6% of Fe by Mn in $La_{0.8}Y_{0.2}(Fe,Mn)AsO_{0.85}F_{0.15}$.

C. Magnetic properties of the 0.5% Mn series

Four selected magnetic volume susceptibility measurements on samples with 1, 5, 10, and 15% Y are shown in Fig. 9 to illustrate the general trend in the response of the system to Y substitution. The susceptibility measurements of all superconductive samples can be found in the Supplemental Material [24]. In contrast to optimally F-doped Y-free La1111, where superconductivity disappears already with 0.2% Mn [1], here the sample with the lowest Y substitution level (0.25%) already shows spurious superconductivity. The samples with 5, 10, and 15% Y show bulk superconductivity with critical temperatures of up to 26 K. This affirms the aforementioned scenario that Mn has a poisoning effect on superconductivity, but Y has a healing effect. The critical temperatures of the whole series are plotted in Fig. 10. The error bars in this graph are obtained by comparing two samples with the same nominal composition; the error becomes smaller with increasing Y as the Y content gets easier to control. With increasing Y content T_c is increasing in an asymptotical way. The effects of the difficult stoichiometry control as mentioned in Sec. IV A can be observed here as well—a large scatter of T_c can be seen in samples with Y contents below 1%. But the large scattering of T_c for small Y contents still gives important information—very small changes in stoichiometry lead to pronounced changes in the physical properties, which may be hinting at this system being near a quantum critical point as has been suggested by Hammerath *et al.* [15]

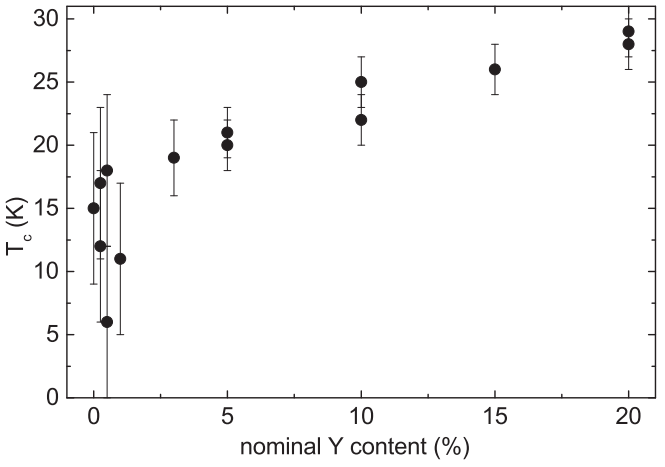

FIG. 10. Critical temperatures of the 0.5% Mn series obtained by susceptibility measurements plotted against the nominal Y content. The error bars are obtained from the comparison of two samples with the same nominal composition.

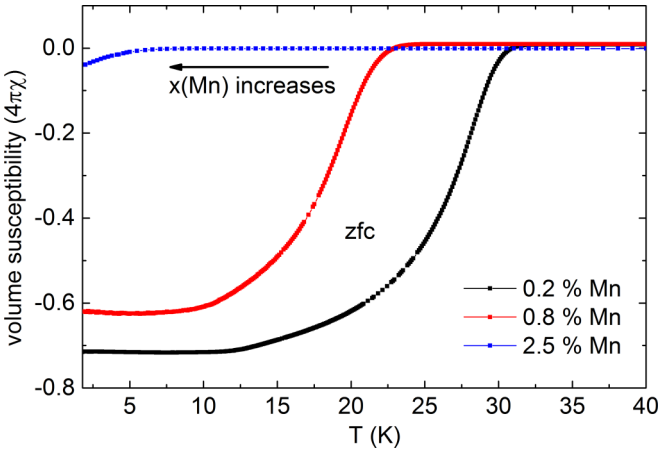

FIG. 11. Magnetic volume susceptibility measured with a field of 10–20 Oe of three samples of the 20% Y series with 0.2, 0.8, 2.5% Mn without demagnetization correction.

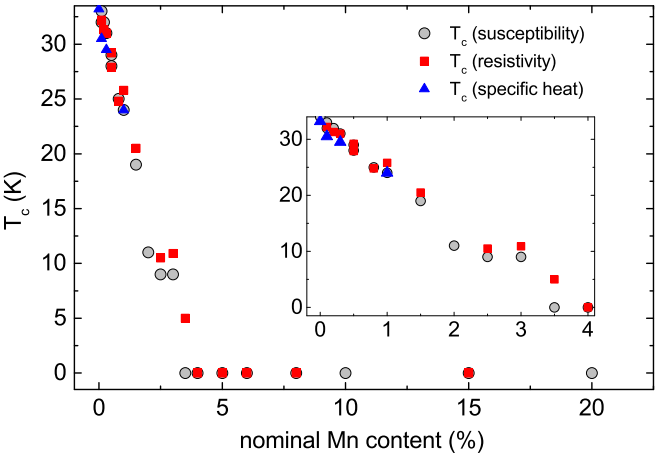

FIG. 13. Critical temperatures of the 20% Y series obtained by susceptibility measurements (gray), resistivity measurements (red), and specific heat measurements (blue) plotted as a function of the nominal Mn content. The inset shows the superconducting region.

A ferromagnetic transition stemming from a ferromagnetic second phase (probably $LaMnO_3$ [29]) can be observed in many samples in susceptibility measurements at 1 T. As this secondary phase cannot be detected using XRD and EDX, we estimate the amount to be smaller than 0.5 wt%. This impurity has also been reported in Y-free Mn-substituted La1111 [28].

D. Magnetic properties of the 20% Y series

Figure 11 shows the magnetic volume susceptibility of three selected samples with 0.2, 0.8, and 2.5% Mn as a function of the temperature. The susceptibility measurements of all superconducting samples can be found in the Supplemental Material [24]. The samples with small Mn contents show bulk superconductivity, but the superconducting volume fraction decreases with increasing Mn content as shown in Fig. 12. The critical temperatures of the whole series are plotted in Fig. 13. In this sample series, we also observed a ferromagnetic transition of a tiny amount of a $LaMnO_3$ impurity phase in high external magnetic fields of 1 T as mentioned in Sec. IV C.

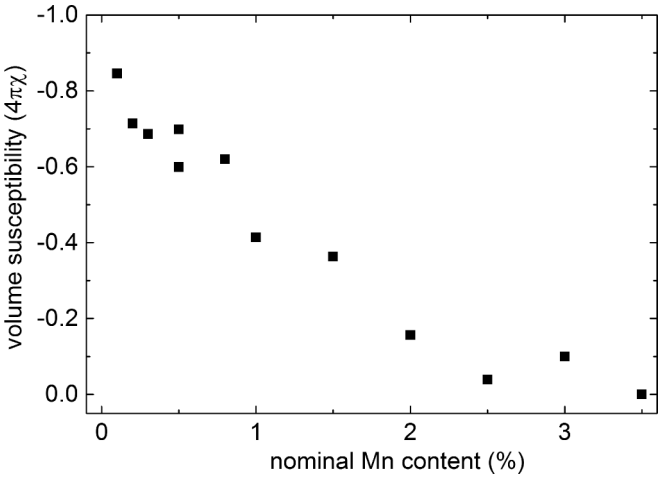

FIG. 12. Relative volume susceptibility measured at 2 K as function of Mn content for the superconducting samples of the 20% Y series (without demagnetization correction).

E. Specific heat results of the 20% Y series

The specific heat capacity of selected samples of the 20% Y series was studied as a function of temperature in zero field and in an external field of 9 T. The c_p/T versus T plots do not show a sharp and clear anomaly at T_c, which indicates possible disorder causing inhomogeneous superconducting states broadening the expected transition. This, however, is quite common for polycrystalline superconducting La1111 samples [30–32] and is similarly present for purely F-doped La1111.

In order to obtain a reasonable estimate for T_c as well as for the Sommerfeld coefficient for our samples, we subtracted the specific heat in an external field of 9 T from the zero-field specific heat. This approach assumes that the superconducting transition is mainly suppressed and slightly shifted to lower temperatures in high magnetic fields, so that the specific heat is mainly described by phononic contributions and the conduction electrons in the normal state. The difference of the specific heat $\Delta c_p/T$ in zero field and 9 T is shown in Fig. 14 for several doping levels of Mn ($0 \leqslant x_{Mn} \leqslant 1\%$). A clear anomaly is visible for all four samples, proving the high quality of our septenary system, which is a remarkable result as such.

The superconducting transition temperature T_c of four selected superconducting samples was determined using an entropy-balance construction which is exemplarily shown for the 0% Mn sample in the inset of Fig. 14. The values for T_c match nicely with the ones obtained from magnetization, and resistivity measurements as visible in the phase diagram in Fig. 13.

We derived the Sommerfeld coefficient γ in two different ways. Usually one plots the specific heat as c_p/T versus T^2 for $T > T_c$, following $c_{el} + c_{ph} = \gamma T + \beta T^3$ with γ and β as the electronic and lattice coefficients. The high values for T_c around 30 K, however, prevent us from this approach. Therefore, for the superconducting samples depicted in Fig. 14,

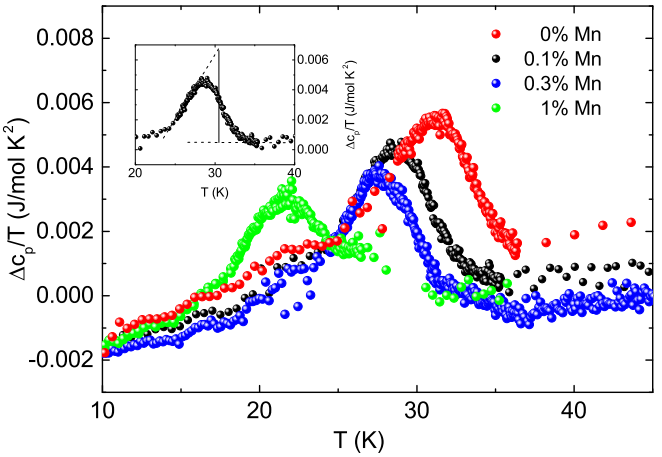

FIG. 14. The difference of the specific heat heat $\Delta c_p/T$ in zero field and 9 T as a function of temperature for several samples within the 20% Y series. The inset exemplarily depicts the entropy-balance construction for the $x_{Mn} = 0$ sample.

we estimated the Sommerfeld coefficients from the jump magnitudes Δc_p at T_c using the relation $\Delta c_p/T = 1.43\,\gamma$ from BCS theory as a first approximation. The obtained values for small Mn contents, shown in Table I, are on the same order of magnitude as purely fluorine-doped La1111 samples [30–32], however, a clear trend can be observed with a slightly increasing Sommerfeld coefficient upon Mn substitution.

For the non-fully-superconducting samples, the Sommerfeld coefficient was estimated by fitting the above mentioned equation $c_p/T = \gamma + \beta T^3$ to the experimental data for 5 K $< T <$ 12 K. Note that the extracted γ values might suffer from a small systematic error, i.e., result in a slight overestimation of γ due to possible magnetic impurities. In the fitting procedure, the observable upturn in the specific heat below 5 K was neglected though (not shown). The obtained values are also shown in Table I.

F. Resistivity as a function of T and Mn content in the 20% Y series

In the resistivity measurements, three distinctive features can be assigned: Some samples show superconducting behavior where the resistivity drops to zero (T_c), some samples exhibit a local minimum ($T_{\min}$), all samples display an inflection point ($T_{\text{inflection}}$) at higher temperatures, the latter two hinting at changes in the electronic structure [33,34]. $T_{\text{inflection}}$ was determined using the second derivative $\frac{d^2\rho}{dT^2}$.

TABLE I. Sommerfeld coefficients γ of several samples of the 20% Y series.

x(Mn) in %	γ in mJ/mol K^2%
0	3.5(2)
0.1	4.1(2)
0.3	4.2(2)
1	4.0(5)
2.5	8.0(5)
3.5	8.7(5)
4	9.0(5)

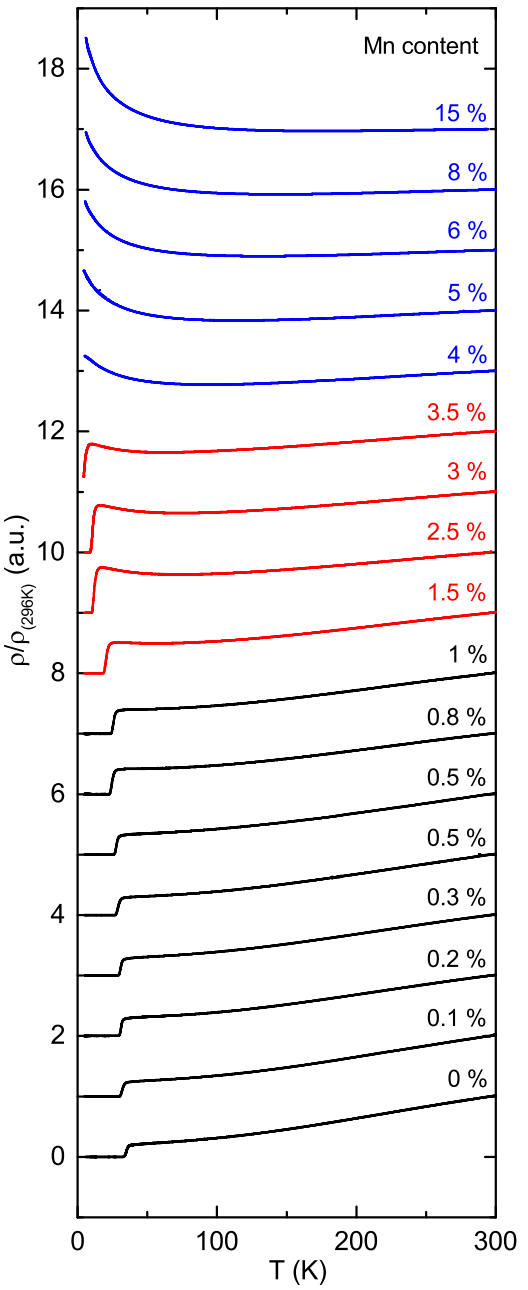

FIG. 15. Resistivity measurements on all samples of the 20% Y series. The measurements in black show samples that only show superconductivity; the red curves are used for samples which show superconductivity and also a local minimum. The blue curves correspond to samples showing a local minimum but no superconductivity. The sample with 3.5% Mn only shows the onset of the resistivity drop but no full superconductivity.

In the 20% Y series, all samples with a Mn content of less than 3.5% show superconductivity as seen in Fig. 15. Samples with a Mn between 1.5 and 3.5% show superconductivity and also a local minimum indicating localization effects. The sample with 3.5% Mn shows an onset of superconductivity but does not become fully superconducting. This is consistent

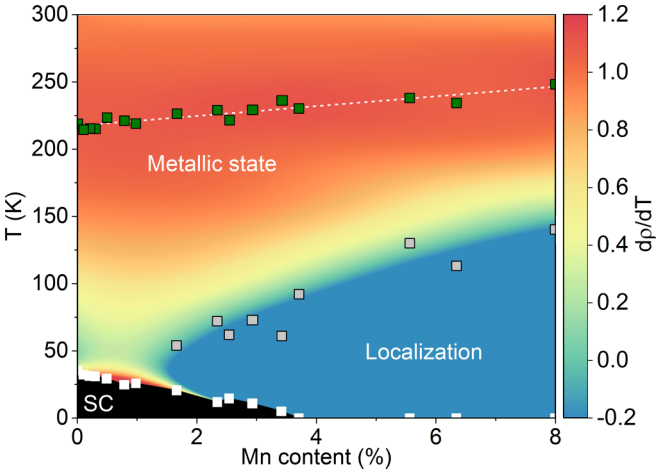

FIG. 16. Phase diagram according to resistivity measurements of the 20% Y series. The first derivative of the resistivity (normalized to room temperature) is plotted versus T and x(Mn). The black area is the superconducting region, in blue parts $\frac{d\rho}{dT}$ is below zero, in red parts $\frac{d\rho}{dT}$ is above 1. T_c is marked with white squares, T_{min} is shown using gray squares, the green squares correspond to $T_{\text{inflection}}$. The dashed line shows the increase of $T_{\text{inflection}}$.

with the magnetization measurement on this sample where no superconductivity could be observed (taking percolation effects into account). The nonsuperconducting samples show an upturn at low temperatures, also highlighting the electron localization caused by Mn. The resistivity measurements complement the magnetization results quite nicely as shown in Fig. 13 where T_c obtained from both methods is plotted against the nominal Mn content.

Changes in the electronic structure of local charge carriers manifest in changes in resistivity, so to gain further insight, the first derivative of the resistivity $\frac{d\rho}{dT}$ is plotted against the Mn content and the temperature in Fig. 16. In the black area the samples show superconducting behavior, in the yellow to orange areas $\frac{d\rho}{dT}$ is below 1, and in the red areas $\frac{d\rho}{dT}$ is above 1, also in the blue area $\frac{d\rho}{dT}$ is below zero. $T_{\text{inflection}}$ is increasing with increasing Mn content.

G. Mößbauer measurements on the 20% Y series

Mößbauer measurements were carried out at room temperature and at 4.2 K on selected samples to check for changes in the spin state of Fe as reaction to Mn substitution, as the unusual structural behavior in the Mn substituted Ba122 system [25] has been attributed to a low spin/high spin transition. Here we use both the isomer shift IS (with respect to room temperature α-Fe) and quadrupole splitting QS to monitor the Fe spin state. As shown in Fig. 17 the spectra consist of a barely split doublet with only minor but noticeable differences in the hyperfine parameters. The spectra were analyzed in terms of quadrupole interaction (with an axial symmetric electric field gradient) using a transmission integral fit with an effective thickness between 0.25 and 0.68.

We observe a significant increase in IS with increasing Mn content (Fig. 18). For two selected samples with 0.8 and 15% of Mn the trend was reproduced at 4.2 K proving similar

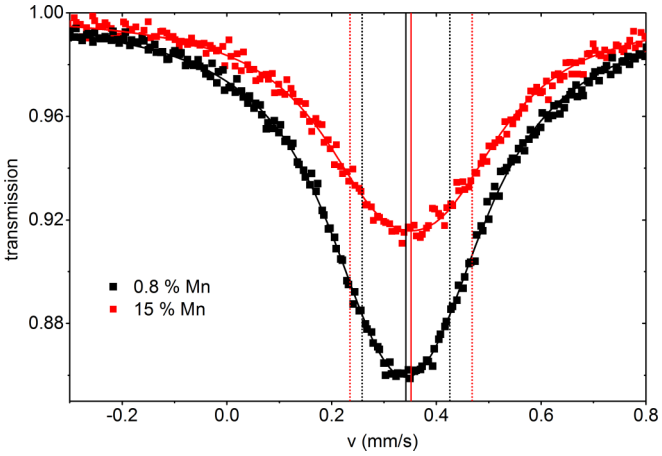

FIG. 17. Mößbauer spectra of two samples of the 20% Y series at room temperature. Quadrupolar splitting (dotted vertical lines) and the center shift (solid vertical lines) increases with Mn content.

Debye temperatures of $\Theta_D \approx 350(5)$ K, which shows that the room temperature measurements are indicative of the chemical shift rather than changes in lattice. Despite the (La,Y)- and (O,F)-substitution the low temperature values $IS(T \to 0) \approx 0.59$ mm/s are on the same order of magnitude as for the parent compound LaFeAsO [35]. The overall increase of IS points to electron localization caused by Mn, but a clear change of valence cannot be observed.

V. DISCUSSION

Coming back to the premise of this paper—can chemical pressure induced by yttrium lead to an increased Mn tolerance in LaFeAs(O,F)? We are able to answer this question with certainty after producing two sample series—first, in the $La_{1-y}Y_yFe_{0.995}Mn_{0.005}AsO_{0.89}F_{0.11}$ (0.5% Mn) series, superconductivity was successfully reinstated by introducing Y to the system up to a maximum of 20% which lead to an increase in T_c up to 32 K. Since samples with the same x(Mn)

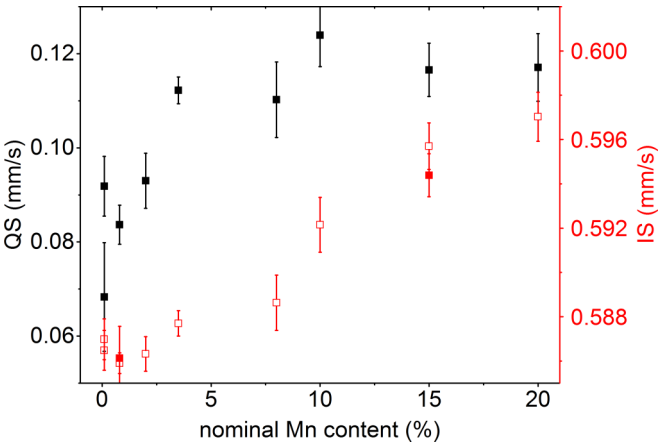

FIG. 18. Mößbauer hyperfine parameters of the 20% Y series: quadrupole splitting (QS, black) and isomer shift (IS, red, the filled squares correspond to measurements at 4.2 K). The systematic change is attributed to an electron localizing effect with increasing Mn content.

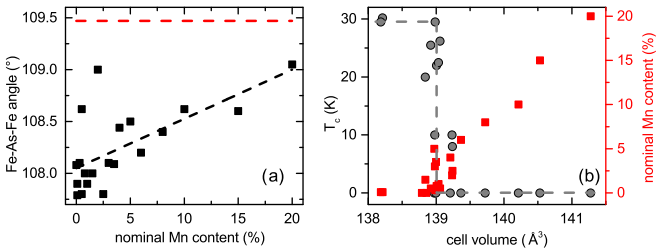

FIG. 19. (a) Fe-As-Fe angle (the red line represents the ideal tetrahedron angle of 109.47°), (b) T_c as a function of the cell volume, both (a) and (b) for the 20% Y series. The dotted line in (b) is added as a guide for the eye.

and a different x(Y) show a different T_c, we can attribute this healing effect to Y. However, it should be noted that in this sample series two Y-free samples with a Mn content of nominally 0.5% still showed superconductivity, a somewhat larger amount than the poisonous 0.2% Mn reported by Sato *et al.* [1]. This different behavior can be explained as noted in Sec. IV C—at this very small substitution level the exact composition is not verifiable using EDX and has a proportionally large error stemming from the fact that only very small amounts of precursors are used in the synthesis.

In a second sample series with 20% Y on the La site, Mn was gradually introduced into the system. The isovalent substitution of La by the much smaller Y ions increases the chemical pressure on the structure and accordingly the hopping integrals in the FeAs layers, causing an effective reduction of the electronic correlations and of the spin polarization around Mn impurities [9,36], resulting in a drastically larger amount of Mn needed to completely quench superconductivity. Superconductivity gets suppressed at about 3.5% Mn, which is an order of magnitude more than the 0.2% Mn that are enough to suppress superconductivity in Y-free LaFeAs(O,F) according to Sato *et al.* [1]. This places the Mn tolerance of (La,Y)FeAs$O_{0.89}F_{0.11}$ close to the one of Nd1111 (4% [1]). As $(La_{0.8}Y_{0.2})^{3+}$ has a hypothetic combined ionic radius of 113 pm, close to Nd^{3+} (111 pm [23]), it is reasonable to conclude that in general, the Mn tolerance of the 1111 systems is relying mostly on the rare earth size.

Having established the healing effect of Y, we now will aim to further shed light on its origin. Since Y induces chemical pressure, this impact should manifest in structural properties. Hence, several relevant structural parameters of the 20% Y series are shown in Fig. 19. The Fe-As-Fe angle as a function of the nominal Mn content shows a linear trend approaching the ideal tetrahedron angle of 109.47° with increasing Mn substitution level, which is unexpected as it has been hypothesized that T_c is getting higher as the Fe-As-Fe angle gets close to this value [37], which is clearly not the case for our study.

Additionally, the critical temperature is plotted as a function of the cell volume in Fig. 19(b). We added the corresponding Mn substitution levels for the sake of clarity. Those graphs indicate a critical volume threshold for the observation of superconductivity—samples with a cell volume of less than 139 $Å^3$ or a corresponding Fe-Fe distance of more than 2.83 Å, have a high T_c; for larger volumes a sharp drop in T_c occurs and samples above this threshold show no superconductivity.

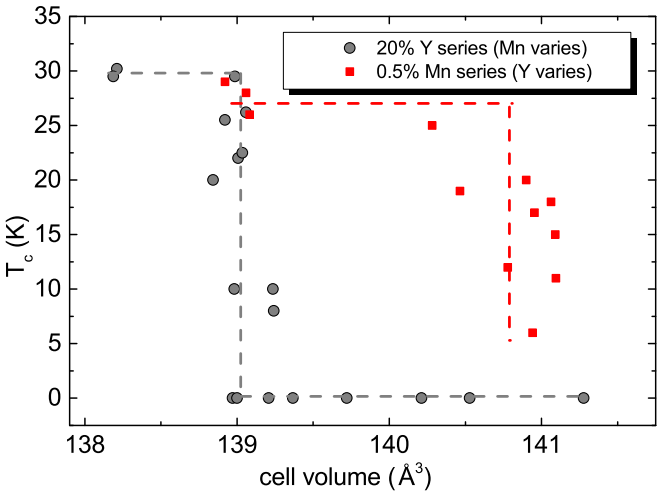

FIG. 20. T_c plotted as a function of the cell volumes for both sample series. The dotted lines are added as a guide for the eye.

To understand the volume threshold for superconductivity, we compared the two sample series to see if this effect is purely correlated to the lattice size—Mn increases the cell volume, Y decreases the cell volume, so one could assume that the respective effect on superconductivity is of a purely steric nature. However, as seen in Fig. 20, this is not the case. Both sample series exhibit a "cutoff" for superconductivity at a certain cell volume, but this cutoff occurs at different values. This suggests a not purely steric effect of Mn on this system.

Mößbauer measurements were conducted to check for a low spin/high spin transition (which might explain the volume threshold) of Fe since the isomer shift IS and the quadrupole splitting QS are both sensitive to the valence and spin state of iron. However, the tetragonal environment and itinerant character of Fe in the given materials conflicts with such a clear low-spin/high-spin picture. Mößbauer measurements showed indeed an increase of IS and QS but not on the order of magnitude one would expect for a classical low spin/high spin transition. Another possible explanation of this threshold may be the onset of populating an antibonding band. The change of IS also reinforces the picture of electron localization by Mn as it confirms the bond length increase in the Fe environment [38,39]. Furthermore, the increase in QS is likely caused by a redistribution of density of states (DOS) in the d states, which results in a higher field gradient V_{zz} value overcompensating possible bond length effects [39]. Remarkably, this is the opposite trend as what has been observed for the ^{75}As NQR frequency in Mn-doped LaFeAs$O_{0.89}F_{0.11}$ where the quadrupole frequency shifts to lower values [9]. This could indicate an electron transfer in our case from As to Fe. Additionally, the increase in QS as seen in Fig. 18 shows a change in steepness around the amount of Mn where superconductivity becomes fully suppressed, suggesting that the suppression of T_c is driven by the redistribution of the DOS among the d states which seems to be connected to the localization process.

To further understand the electronic properties, a closer look at the transport properties is necessary. Resistivity studies show two telling features: a local minimum (present in samples with a Mn content above 1%)—which shifts to higher

temperatures with higher Mn content—and an inflection point at temperatures above 200 K in all samples, which also slightly increases with x(Mn), but decreases with x(Y). This inflection point indicates that magnetic and nematic fluctuations [40] related to the SDW state are still present in all samples, in line with previous NMR results [15,16]. The local minimum and therefore the electron localization is negatively correlated with T_c—samples with very small Mn content do not show the localization effect, but as the Mn content rises, T_c gets shifted to lower temperatures; the local minimum starts to appear at a Mn content of 1.5% and shifts to higher temperatures. A similar effect can be observed in Mn-free $LaFeAsO_{1-x}F_x$ where the parent compound shows an upturn at low temperatures and underdoped samples show a local minimum, signifying the localization of charge carriers [40], which means that this effect is not limited to Mn-containing samples.

To add, the γ values extracted from the specific heat measurements of the 20% Y series are considerably smaller than the ones extracted for purely F/Mn doped $LaFe_{1-x}Mn_xAsO_{0.89}F_{0.11}$ in Ref. [32], where a similar extrapolation method was used to obtain the Sommerfeld coefficient as a function of doping. This could hint towards Y changing the DOS compared to purely F/Mn doping in the La1111 system as already suggested by Mößbauer spectroscopy. In the future, band structure calculations could help in order to disentangle the pure charge carrier effect from other effects such as, e.g., the localization due to the introduced Mn.

VI. SUMMARY AND CONCLUSIONS

We have successfully synthesized high quality polycrystalline samples of $LaFeAsO_{0.89}F_{0.11}$ where La was substituted with Y and Fe was substituted with Mn, therefore constituting a septimal system which is a remarkable result as such. In optimally F doped LaFeAsO, Mn substitution on the Fe position leads to suppression of superconductivity even at a substitution level of only 0.2%, whereas in samples where 20% of La was substituted by Y, superconductivity was only fully suppressed at a Mn substitution level of 3.5%. This shows that inflicting chemical pressure by Y substitution drives the system further away from a quantum critical point in regards of Mn substitution. Mn does not act as a hole dopant but instead leads to electron localization as evidenced in resistivity and Mößbauer measurements.

ACKNOWLEDGMENTS

The authors thank R. Wachtel, D. Meiler, C. G. F. Blum, L. Giebeler, S. Drechsler, S. Müller-Litvanyi, G. Kreutzer, and S. Gass for support. This work has been supported by the Deutsche Forschungsgemeinschaft through the Priority Programme SPP1458 (Grants No. BE1749/13, No. BU887/15), coordinated research center SFB 1143, under Grant No. DFG-GRK1621 and through the Emmy Noether Programme WU595/3-3 (S.W.). Additional funding was received by MIUR-PRIN2015 Project No. 2015C5SEJJ.

[1] M. Sato, Y. Kobayashi, S. C. Lee, H. Takahashi, E. Satomi, and Y. Miura, Studies on effects of impurity doping and NMR measurements of La 1111 and/or Nd 1111 Fe-Pnictide superconductors, J. Phys. Soc. Jpn. **79**, 014710 (2010).

[2] A. Thaler, H. Hodovanets, M. S. Torikachvili, S. Ran, A. Kracher, W. Straszheim, J. Q. Yan, E. Mun, and P. C. Canfield, Physical and magnetic properties of $Ba(Fe_{1-x}Mn_x)_2As_2$ single crystals, New J. Phys. **84**, 144528 (2011).

[3] D. Kasinathan, A. Ormeci, K. Koch, U. Burkhardt, W. Schnelle, A. Leithe-Jasper, and H. Rosner, AFe_2As_2 (A = Ca, Sr, Ba, Eu) and $SrFe_{2-x}TM_xAs_2$ (TM = Mn, Co, Ni): crystal structure, charge doping, magnetism and superconductivity, New J. Phys. **11**, 025023 (2009).

[4] M. Rotter, M. Tegel, and D. Johrendt, Superconductivity at 38 K in the Iron Arsenide $(Ba_{1-x}K_x)Fe_2As_2$, Phys. Rev. Lett. **101**, 107006 (2008).

[5] Y. Texier, Y. Laplace, P. Mendels, K. T. Park, G. Friemel, D. L. Sun, D. S. Inosov, C. T. Lin, and J. Bobroff, Mn local moments prevent superconductivity in iron pnictides $Ba(Fe_{1-x}Mn_x)_2As_2$, Europhys. Lett. **99**, 17002 (2012).

[6] D. S. Inosov, G. Friemel, J. T. Park, A. C. Walters, Y. Texier, Y. Laplace, J. Bobroff, V. Hinkov, D. L. Sun, Y. Liu, R. Khasanov, K. Sedlak, Ph. Bourges, Y. Sidis, A. Ivanov, C. T. Lin, T. Keller, and B. Keimer, Possible realization of an antiferromagnetic Griffiths phase in $Ba(Fe_{1-x}Mn_x)_2As_2$, Phys. Rev. B **87**, 224425 (2013).

[7] H. Suzuki, T. Yoshida, S. Ideta, G. Shibata, K. Ishigami, T. Kadono, A. Fujimori, M. Hashimoto, D. H. Lu, Z.-X. Shen, K. Ono, E. Sakai, H. Kumigashira, M. Matsuo, and T. Sasagawa, Absence of superconductivity in the hole-doped Fe pnictide $Ba(Fe_{1-x}Mn_x)_2As_2$: Photoemission and x-ray absorption spectroscopy studies, Phys. Rev. B **88**, 100501(R) (2013).

[8] S. Singh, J. Shimoyama, A. Yamamoto, H. Ogino, and K. Kishio, Effects of Mn and Ni doping on the superconductivity of SmFeAs(O, F), Physica C **494**, 57 (2013).

[9] M. Moroni, P. Carretta, G. Allodi, R. De Renzi, M. N. Gastiasoro, B. M. Andersen, P. Materne, H.-H. Klauss, Y. Kobayashi, M. Sato, and S. Sanna, Fast recovery of the stripe magnetic order by Mn/Fe substitution in F-doped LaFeAsO superconductors, Phys. Rev. B **95**, 180501 (2017).

[10] G. Lamura, T. Shiroka, S. Bordignon, S. Sanna, M. Moroni, R. De Renzi, P. Carretta, P. K. Biswas, F. Caglieris, M. Putti, S. Wurmehl, S. J. Singh, J. Shimoyama, M. N. Gastiasoro, and B. M. Andersen, Role of magnetic dopants in the phase diagram of Sm 1111 pnictides: The case of Mn, Phys. Rev. B **94**, 214517 (2016).

[11] J. M. Lock, The magnetic susceptibilities of Lanthanum, Cerium, Praseodymium, Neodymium and Samarium, from 1.5 K to 300 K, Proc. Phys. Soc. London, Sect. B **70**, 566 (1957).

[12] P. M. Shirage, K. Miyazawa, H. Kito, H. Eisaki, and A. Iyo, Superconductivity at 43 K at ambient pressure in the iron-based layered compound $La_{1-x}Y_xFeAsO_y$, Phys. Rev. B **78**, 172503 (2008).

[13] M. Tropeano, C. Fanciulli, F. Canepa, M. R. Cimberle, C. Ferdeghini, G. Lamura, A. Martinelli, M. Putti, M. Vignolo, and A. Palenzona, Effect of chemical pressure on spin density

wave and superconductivity in undoped and 15% F-doped $La_{1-y}Y_yFeAsO$ compounds, Phys. Rev. B **79**, 174523 (2009).

[14] H. Takahashi, K. Igawa, K. Arii, Y. Kamihara, M. Hirano, and H. Hosono, Superconductivity at 43 K in an iron-based layered compound $LaO_{1-x}F_xFeAs$, Nature (London) **453**, 376 (2008).

[15] F. Hammerath, P. Bonfà, S. Sanna, G. Prando, R. De Renzi, Y. Kobayashi, M. Sato, and P. Carretta, Poisoning effect of Mn in $LaFe_{1-x}Mn_xAsO_{0.89}F_{0.11}$: Unveiling a quantum critical point in the phase diagram of iron-based superconductors, Phys. Rev. B **89**, 134503 (2014).

[16] F. Hammerath, M. Moroni, L. Bossoni, S. Sanna, R. Kappenberger, S. Wurmehl, A. U. B. Wolter, M. A. Afrassa, Y. Kobayashi, M. Sato, B. Büchner, and P. Carretta, Enhancement of low-frequency fluctuations and superconductivity breakdown in Mn-doped $La_{1-y}Y_yFeAsO_{0.89}F_{0.11}$ superconductors, Phys. Rev. B **92**, 020505 (2015).

[17] M. Moroni, S. Sanna, G. Lamura, T. Shiroka, R. De Renzi, R. Kappenberger, M. A. Afrassa, S. Wurmehl, A. U. B. Wolter, B. Büchner, and P. Carretta, Competing effects of Mn and Y doping on the low-energy excitations and phase diagram of $La_{1-y}Y_yFe_{1-x}Mn_xAsO_{0.89}F_{0.11}$ iron-based superconductors, Phys. Rev. B **94**, 054508 (2016).

[18] A. Alfonsov, F. Murányi, V. Kataev, G. Lang, N. Leps, L. Wang, R. Klingeler, A. Kondrat, C. Hess, S. Wurmehl, A. Köhler, G. Behr, S. Hampel, M. Deutschmann, S. Katrych, N. D. Zhigadlo, Z. Bukowski, J. Karpinski, and B. Büchner, High-field electron spin resonance spectroscopy study of $GdFeAsO_{1-x}F_x$ superconductors, Phys. Rev. B **83**, 094526 (2011).

[19] H. M. Rietveld, A profile refinement method for nuclear and magnetic structures, J. Appl. Crystallogr. **2**, 65 (1969).

[20] T. Roisnel, and J. Rodríquez-Carvajal, WinPLOTR: A Windows Tool for Powder Diffraction Pattern Analysis, Mater. Sci. Forum **378**, 118 (2001).

[21] S. Kamusella, and H.-H. Klauss, Moessfit, Hyperfine Interact. **237**, 82 (2016).

[22] L. Vegard, Die Konstitution der Mischkristalle und die Raumfüllung der Atome, Z. Phys. **5**, 17 (1921).

[23] R. D. Shannon, Revised Effective Ionic Radii and Systematic Studies of Interatomic Distances in Halides and Chalcogenides, Acta Crystallogr. A **32**, 751 (1976).

[24] See Supplemental Material at http://link.aps.org/supplemental/10.1103/PhysRevB.97.054522 for all Rietveld refinement and magnetization measurements.

[25] A. Thaler, H. Hodovanets, M. S. Torikachvili, S. Ran, A. Kracher, W. Straszheim, J. Q. Yan, E. Mun, and P. C. Canfield, Physical and magnetic properties of $Ba(Fe_{1-x}Mn_x)_2As_2$ single crystals, Phys. Rev. B **84**, 144528 (2011).

[26] F. Steckel, M. Roslova, R. Beck, I. Morozov, S. Aswartham, D. Evtushinsky, C. G. F. Blum, M. Abdel-Hafiez, D. Bombor, J. Maletz, S. Borisenko, A. V. Shevelkov, A. U. B. Wolter, C. Hess, S. Wurmehl, and B. Büchner, Crystal growth and electronic phase diagram of 4*d*-doped $Na_{1-\delta}Fe_{1-x}Rh_xAs$ in comparison to 3*d*-doped $Na_{1-\delta}Fe_{1-x}Co_xAs$, Phys. Rev. B **91**, 184516 (2015).

[27] D. Johrendt, Structure-property relationships of iron arsenide superconductors, J. Mater. Chem. **21**, 13726 (2011).

[28] R. Frankovsky, H. Luetkens, F. Tambornino, A. Marchuk, G. Pascua, A. Amato, H.-H. Klauss, and D. Johrendt, Short-range magnetic order and effective suppression of superconductivity by manganese doping in $LaFe_{1-x}Mn_xAsO_{1-y}F_y$, Phys. Rev. B **87**, 174515 (2013).

[29] G. Matsumoto, Study of $(La_{1-x}Ca_x)MnO_3$. I. Magnetic Structure of $LaMnO_3$, J. Phys. Soc. Jpn. **29**, 606 (1970).

[30] A. S. Sefat, M. A. McGuire, B. C. Sales, R. Jin, J. Y. Howe, and D. Mandrus, Electronic correlations in the superconductor $LaFeAsO_{0.89}F_{0.11}$ with low carrier density, Phys. Rev. B **77**, 174503 (2008).

[31] Y. F. Guo, Y. G. Shi, S. Yu, A. A. Belik, Y. Matsushita, M. Tanaka, Y. Katsuya, K. Kobayashi, I. Nowik, I. Felner, V. P. S. Awana, K. Yamaura, and E. Takayama-Muromachi, Large decrease in the critical temperature of superconducting $LaFeAsO_{0.85}$ compounds doped with 3% atomic weight of nonmagnetic Zn impurities, Phys. Rev. B **82**, 054506 (2010).

[32] T. Kawamata, E. Satomi, Y. Kobayashi, M. Itoh, and M. Sato, Study of Ni-Doping Effect of Specific Heat and Transport Properties for $LaFe_{1-y}Ni_yAsO_{0.89}F_{0.11}$, J. Phys. Soc. Jpn. **80**, 084720 (2011).

[33] Y. Ando, S. Komiya, K. Segawa, S. Ono, and Y. Kurita, Electronic Phase Diagram of High-T_c Cuprate Superconductors from a Mapping of the In-Plane Resistivity Curvature, Phys. Rev. Lett. **93**, 267001 (2004).

[34] C. Hess, A. Kondrat, A. Narduzzo, J. E. Hamann-Borrero, R. Klingeler, J. Werner, G. Behr, and B. Büchner, The intrinsic electronic phase diagram of iron-oxypnictide superconductors, Europhys. Lett. **87**, 17005 (2009).

[35] M. A. McGuire, A. D. Christianson, A. S. Sefat, B. C. Sales, M. D. Lumsden, R. Jin, E. A. Payzant, D. Mandrus, Y. Luan, V. Keppens, V. Varadarajan, J. W. Brill, R. Hermann, M. T. Sougrati, F. Grandjean, and G. J. Long, Phase Transitions in LaFeAsO: Structural, Magnetic, Elastic, and Transport Properties, Heat Capacity and Mössbauer Spectra, Phys. Rev. B **78**, 094517 (2008).

[36] M. N. Gastiasoro, F. Bernardini, and B. M. Andersen, Unconventional Disorder Effects in Correlated Superconductors, Phys. Rev. Lett. **117**, 257002 (2016).

[37] S. A. J. Kimber, A. Kreyssig, Y.-Z. Zhang, H. O. Jeschke, R. Valenti, F. Yokaichiya, E. Colombier, J. Yan, T. C. Hansen, T. Chatterji, R. J. McQueeney, P. C. Canfield, A. I. Goldman, and D. N. Argyriou, Similarities between structural distortions under pressure and chemical doping in superconducting $BaFe_2As_2$, Nat. Mater. **8**, 471 (2009).

[38] Z. Li, Y. Fang, X. Ma, H. Pang, and F. Li, Charge redistribution at the antiferromagnetic phase transition in the SrFeAsF compound, Phys. Rev. B **84**, 134509 (2011).

[39] S. L. Bud'ko, X. Ma, M. Tomić, S. Ran, R. Valentí, and P. C. Canfield, Transition to collapsed tetragonal phase in $CaFe_2As_2$ single crystals as seen by ^{57}Fe Mössbauer spectroscopy, Phys. Rev. B **93**, 024516 (2016).

[40] C. Hess, H. Grafe, A. Kondrat, G. Lang, F. Hammerath, L. Wang, R. Klingeler, G. Behr, and B. Büchner, Nematicity in $LaFeAsO_{1-x}F_x$, Phys. Status Solidi B **254**, 1600214 (2017).